JACS Au
AN OPEN ACCESS JOURNAL OF THE AMERICAN CHEMICAL SOCIETY

pubs.acs.org/jacsau

Article

Expanding Knowledge of Methylotrophic Capacity: Structure and Properties of the Rough-Type Lipopolysaccharide from *Methylobacterium extorquens* and Its Role on Membrane Resistance to Methanol

Flaviana Di Lorenzo,[¶] Simone Nicolardi,[¶] Roberta Marchetti, Adele Vanacore, Noemi Gallucci, Katarzyna Duda, Ferran Nieto Fabregat, Ha Ngoc Anh Nguyen, Djamel Gully, James Saenz, Eric Giraud, Luigi Paduano, Antonio Molinaro, Gerardino D'Errico, and Alba Silipo*

Cite This: *JACS Au* 2023, 3, 929–942

Read Online

ACCESS | Metrics & More | Article Recommendations | Supporting Information

ABSTRACT: The ability of *Methylobacterium extorquens* to grow on methanol as the sole carbon and energy source has been the object of intense research activity. Unquestionably, the bacterial cell envelope serves as a defensive barrier against such an environmental stressor, with a decisive role played by the membrane lipidome, which is crucial for stress resistance. However, the chemistry and the function of the main constituent of the *M. extorquens* outer membrane, the lipopolysaccharide (LPS), is still undefined. Here, we show that *M. extorquens* produces a rough-type LPS with an uncommon, non-phosphorylated, and extensively *O*-methylated core oligosaccharide, densely substituted with negatively charged residues in the inner region, including novel monosaccharide derivatives such as *O*-methylated Kdo/Ko units. Lipid A is composed of a non-phosphorylated trisaccharide backbone with a distinctive, low acylation pattern; indeed, the sugar skeleton was decorated with three acyl moieties and a secondary very long chain fatty acid, in turn substituted by a 3-*O*-acetyl-butyrate residue. Spectroscopic, conformational, and biophysical analyses on *M. extorquens* LPS highlighted how structural and tridimensional features impact the molecular organization of the outer membrane. Furthermore, these chemical features also impacted and improved membrane resistance in the presence of methanol, thus regulating membrane ordering and dynamics.

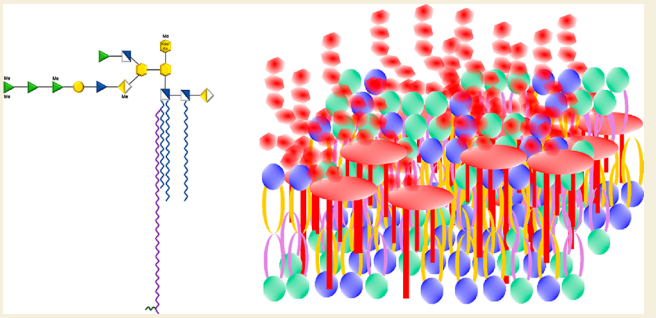

KEYWORDS: *Methylobacterium extorquens, lipopolysaccharide (LPS), lipid bilayers, NMR spectroscopy, ESI FT-ICR mass spectrometry, lipid A MALDI MS, electron paramagnetic resonance (EPR), small-angle neutron scattering (SANS)*

INTRODUCTION

Plant microbiota constitutes a complex co-association of diverse microorganisms, including bacteria, fungi, protists, nematodes, and viruses, able to colonize and proliferate in the assorted multitude of niches furnished by plants.[1,2] The genus *Methylobacterium* includes pink-pigmented facultative Gram-negative methylotrophs belonging to the Rhizobiales family of Alphaproteobacteria. *Methylobacteria* are detected ubiquitously in nature, including soil, dust, lake sediments, and air, besides being considered dominant actors of the plant-associated microbial community.[3] They potentially dominate the phyllosphere population as epiphytic and endophytic leaf colonizers;[4] some representatives associate to plant roots and exhibit a true symbiosis with *Crotalaria* and *Lotononis* plants.[5,6] As methylotrophs, *Methylobacteria* can grow at the expense of methanol (and methylamine), released by plant leaves as a byproduct of pectin metabolism during cell wall synthesis.[7] This unique ability to use methanol as a carbon and energy source provides a selective advantage during colonization under competitive conditions.[8] This becomes even more interesting if one considers that the widespread and productive *Methylobacterium*-plant association is known to accelerate growth and fitness, thus suggesting that bacteria genetic manipulation can be used for plant protection against pathogens and pests.[3,4,9] As a matter of fact, in a number of studies, *Methylobacterium* and, in particular, *M. extorquens* have been engineered for this purpose, but also to produce value-

Received: January 12, 2023
Revised: February 11, 2023
Accepted: February 15, 2023
Published: March 9, 2023

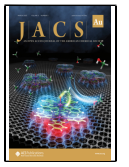

https://doi.org/10.1021/jacsau.3c00025
JACS Au 2023, 3, 929–942

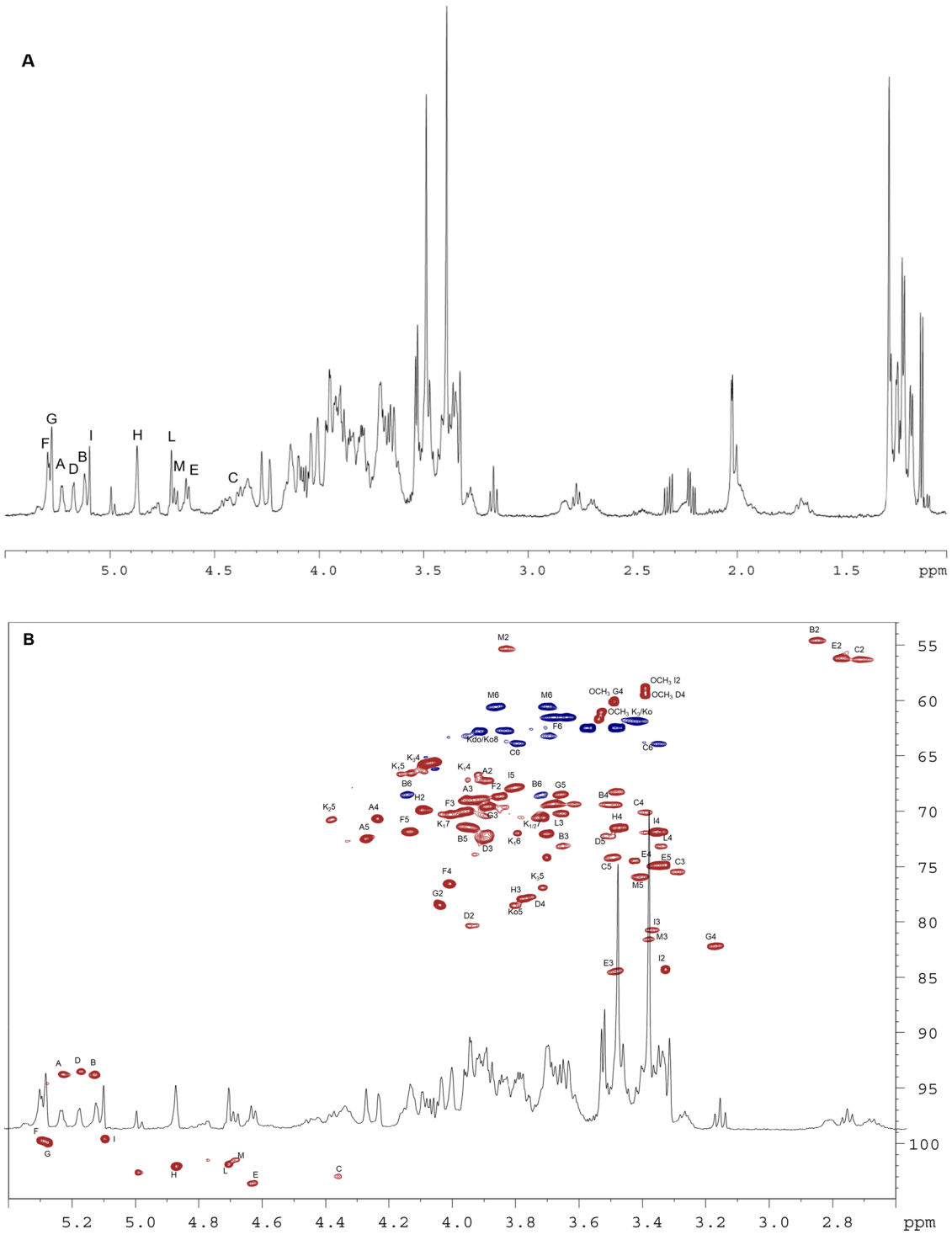

Figure 1. (A) ^{1}H NMR spectrum of *M. extorquens* PA1 $\mathbf{OS_{deAc}}$. Anomeric proton signals are labeled as in Table S1. (B) Multiplicity-edited heteronuclear single-quantum coherence (HSQC) spectrum of *M. extorquens* PA1 $\mathbf{OS_{deAc}}$ (red-colored cross peaks refer to −CH and $-CH_3$ signals, blue-colored ones refer to $-CH_2$ signals). Sugar residues (A−M) are labeled as in Table S1.

added compounds from methanol, which is considered a promising inexpensive substrate for use in the biotechnology industry.[10]

Intrigued by the methylotrophic capacity of this bacterium and in consideration of the role bacterial cell envelope plays as a defensive barrier, we investigated the structure, properties, and role that its main glycoconjugate, lipopolysaccharide (LPS), plays in mediating adaptation to methanol as an environmental stressor/factor.[11−13] LPS is the main component of the external layer of Gram-negative outer membrane; it contributes to viability and mediates interactions with the host and external milieu. LPS is a tripartite macromolecule built up of a glycolipid portion, lipid A, linked to a saccharide moiety, in turn distinguished in an oligosaccharide (core OS) and a polysaccharide portion, the O-antigen.[14] If this last is absent, LPS is defined as rough-type LPS or lipooligosaccharide (LOS). Bacteria can react to the selective pressure of plant/host immunity and withstand environmental threats owing to

https://doi.org/10.1021/jacsau.3c00025
JACS Au 2023, 3, 929−942

the structural adaptability and flexibility of LPS, which is involved in many aspects of host−microbe interactions, either detrimental and beneficial, such as colonization, symbiosis, and virulence.[15−17]

Here, we characterized the structure of the LOS isolated from two *Methylobacterium* strains, *M. extorquens* PA1 and AM1, both competitive colonizers of the phyllosphere of *Arabidopsis thaliana*. We demonstrate that both express an uncommon, non-phosphorylated, and extensively *O*-methylated core OS, which is, however, highly negatively charged due to the presence of a 3-deoxy-D-*manno*-octulosonic acid (Kdo) disaccharide in the inner core region, substituted by a further, terminal ulosonic acid, alternatively constituted by the unreported 5-*O*-methylated D-*glycero*-D-*talo*-2-octulosonic acid (Ko) or Kdo unit. In addition, lipid A consisted of a non-phosphorylated trisaccharide backbone, with a galacturonic acid (GalA) unit located on the distal glucosamine (GlcN) through a trehalose-like α,α-(1 → 1) glycosidic linkage. The lipid A skeleton was characterized by a low acylation pattern, consisting of three lipid moieties directly decorating the backbone and a fourth, secondary very long chain fatty acid (VLCFA) carrying an unprecedented 3-*O*-acetyl-butyrate substitution. We also investigated the role of LOS in stabilizing *M. extorquens* OM, both in water buffer conditions and in the presence of methanol. Biophysical and spectroscopic analyses (i.e., small-angle neutron scattering, SANS, dynamic light scattering, DLS, and electron paramagnetic resonance, EPR) on lipid vesicles indicated that the structural features of *M. extorquens* LOS can stabilize and consolidate the bilayer and induce further lipid ordering when evaluated in the presence of methanol.

RESULTS

M. extorquens LOS Isolation and Chemical Analyses

The LOS from the two *Methylobacterium* strains was isolated from dried bacterial pellet and purified with DNase, RNase, and proteases, followed by dialysis, ultracentrifugation, and gel-filtration chromatography. Compositional analyses highlighted the occurrence of D-glucosamine (D-GlcN), 3-deoxy-D-*manno*-oct-2-ulosonic acid (Kdo), 5-*O*-methyl-Kdo (Kdo5OMe), 5-*O*-methyl-Ko (Ko5OMe), D-galacturonic acid (D-GalA), rhamnose (D-Rha), D-quinovosamine (D-QuiN), and D-galactose (D-Gal). Methylation analysis showed the presence of 6-substituted and 3-substituted GlcN (6-GlcN and 3-GlcN), 2-substituted and terminal GalA (*t*-GalA and 2-GalA), 2,4-substituted, 3-substituted, 2,3-substituted, 2-substituted, and terminal Rha (2,4-Rha, 3-Rha, 2,3-Rha, 2-Rha, and *t*-Rha), 4-substituted Gal (4-Gal), 3-substituted QuiN (3-QuiN), 4,5-disubstituted Kdo (4,5-Kdo), terminal 5-*O*-methyl-Kdo (*t*-Kdo5OMe), and terminal 5-*O*-methyl-Ko (*t*-Ko5OMe); furthermore, a Ko5OMe-(2 → 4)-Kdo disaccharide was also detected (Figure S1). Fatty acid analysis disclosed the occurrence of 14:0(3-OH) and 18:0(3-OH) and 26:0(25-OH) and 28:0(27-OH) as VLCFA.

M. extorquens PA1 and AM1 LOS Structure Determination: NMR Analysis of OS_{deAc}

An aliquot of pure LOS from each strain was fully deacylated to obtain the core oligosaccharide fraction ($\mathbf{OS_{deAc}}$), which in turn was further purified by gel-filtration chromatography. *M. extorquens* PA1 and AM1 $\mathbf{OS_{deAc}}$ then underwent an extensive NMR investigation to assign all spin systems and to establish the saccharide sequence; ^{1}H NMR spectra are reported in Figures 1 and S2. The anomeric configuration of each monosaccharide unit was determined based on the $^3J_{H1,H2}$ coupling constant values, whereas those of vicinal $^3J_{H,H}$ ring coupling constants led to the identification of the relative configuration of each sugar residue. Finally, combined information derived from *inter*-residue nuclear Overhauser effect (NOE) connectivities and heteronuclear long-range correlations, together with compositional analysis, allowed for the complete characterization of both core $\mathbf{OS_{deAc}}$ from *M. extorquens* PA1 and AM1 LOS, which were found to possess the same chemical structure. The NMR spectra revealed the presence of 14 sugar units, all present as pyranose rings, according to both ^{13}C chemical shift values and long-range correlations between C-1/H-1 and H-5/C-5 in the ^{1}H and ^{13}C HMBC spectrum (for the Kdo/Ko residues between C-2 and H-6) (Table S1, Figures 1, and S2−S4).[18]

Spin systems **A**, **B**, and **F** were identified as *galacto* configured sugar units, as indicated by the $^3J_{H3,H4}$ and $^3J_{H4,H5}$ values (3 and <1 Hz, respectively). Both $^3J_{H1,H2}$ and $^1J_{CH}$ coupling constant values, together with *intra*-residual NOE contact of H-1 with H-2, were diagnostic of their α-configurations and $^4C_1$ ring conformation. Furthermore, spin systems **A** and **B** correlated at position 6 to carboxylic groups, allowing for identification of **A** and **D** as GalA residues. Residue **E** was identified as β-QuiN, as attested by the scalar correlations of ring protons to the methyl signal at position 6. The *gluco* configuration of **E** was indicated by the ring $^3J_{H,H}$ coupling constants (8−10 Hz), while in the HSQC spectrum, H-2 resonance correlated to a nitrogen-bearing carbon signal at 56.1 ppm. The *intra*-residual NOE contact of H-1 with H-3 and H-5 and $^3J_{H1,H2}$ and $^1J_{CH}$ values were indicative of β-anomeric configuration. Residues **C** and **M** were identified as GlcN units, with the *gluco* configuration resulting from the $^3J_{H,H}$ coupling constants, while C-2 correlated to a nitrogen-bearing carbon signal, and the anomeric configurations were identified as mentioned above. Spin systems **G**, **H**, **I**, and **L** were identified as α-Rha units, as attested by the scalar correlations of the ring protons with the methyl signal at position 6, visible in the total correlation spectroscopy (TOCSY) spectrum. The *manno* configuration was established by $^3J_{H\text{-}1,H\text{-}2}$ and $^3J_{H\text{-}2,H\text{-}3}$, both below 2 Hz and diagnostic of the H-2 equatorial orientation; the α-anomeric configuration was assigned by the $^1J_{CH}$ coupling constant. Spin system **K** was attributed to the Kdo residue on the basis of the diastereotopic methylene proton signals resonating in the high-field region of the ^{1}H NMR spectrum; on the basis of the H-3 proton chemical shift, it was possible to assign its α-anomeric configuration.[19] Interestingly, two other spin systems were identified and attributed to Kdo and Ko residues (Table S1 and Figure 1), whose location was definitively assessed by the punctual analysis of high-resolution mass spectrometry spectra.

The downfield displacements of chemical shift for **D4**, **G4**, **I2**, **I3**, $\mathbf{K_3}$**5**, and **Ko5** were all ascribable to the presence of methoxy groups, as proven by the NOE and long-range correlations [respectively from the TROESY and heteronuclear multiple bond correlation (HMBC) spectra] of the above-mentioned proton resonances with the corresponding *O*-methyl groups. The glycosylated positions of the sugar units were identified with the downfield shift of carbon resonances (Table S1). The *inter*-residual NOE contacts (Figure S2) together with the long-range correlations derived from the HMBC spectrum allowed to determine the $\mathbf{OS_{deAc}}$ structure, as depicted in the scheme below and in Figure 2. It is worth

https://doi.org/10.1021/jacsau.3c00025
JACS Au 2023, 3, 929−942

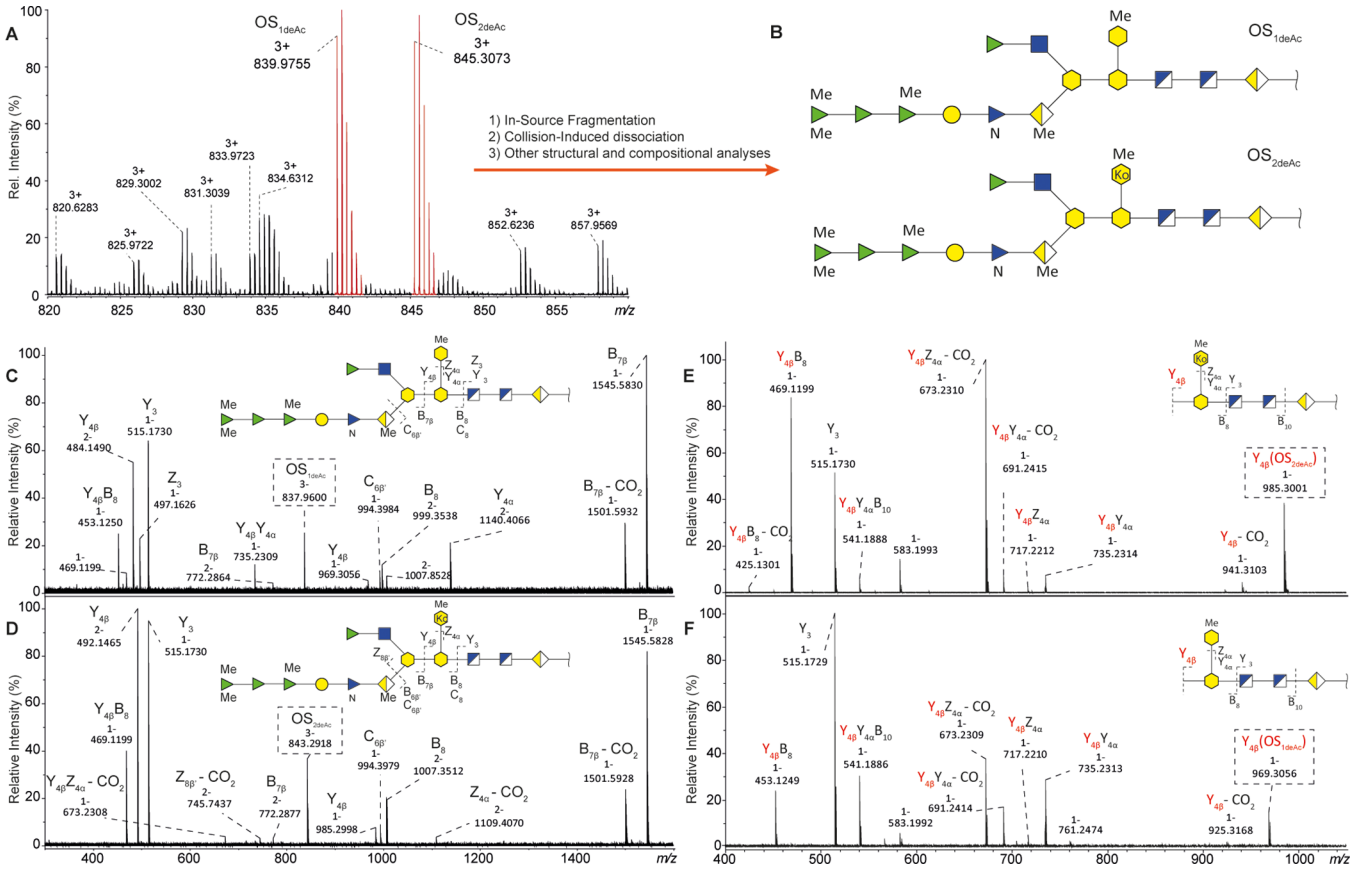

Figure 2. (A) Enlargement of a positive mode electrospray ionization Fourier transform ion cyclotron resonance (ESI FT-ICR) mass spectrum of deacylated LOS ($\mathbf{OS_{deAc}}$). (B) Schematic structures of the two most abundant LOS species identified using an MS-based characterization strategy (see Supporting Information). Symbols legend: green triangle: rhamnose; blue triangle with "N": quinovosamine; yellow/white diamond: galacturonic acid; blue square: *N*-acetyl-glucosamine; blue/white square: glucosamine yellow hexagon: 3-deoxy-D-*manno*-octulosonic acid, Kdo; yellow hexagon with "Ko": D-*glycero*-D-*talo*-2-octulosonic acid, Ko; Me: methylation. (C) Negative mode ESI-CID FT-ICR mass spectrum of deacylated $\mathbf{OS_{1deAc}}$. The deprotonated doubly charged $\mathbf{OS_{1deAc}}$, detected at *m/z* 837.9600, was selected and fragmented by CID in the hexapole collision cell. (D) Negative mode ESI-CID FT-ICR mass spectrum of deacylated $\mathbf{OS_{2deAc}}$. The deprotonated triply charged $\mathbf{OS_{2deAc}}$, detected at *m/z* 843.2918, was selected and fragmented by CID in the hexapole collision cell. (E,F) Negative mode ESI-CID FT-ICR mass spectra of the deprotonated in-source fragments $Y_{4\beta}(\mathbf{OS_{2deAc}})$ and $Y_{4\beta}(\mathbf{OS_{1deAc}})$ detected at *m/z* 985.3001 and *m/z* 969.3056, respectively, and generated using a skimmer voltage of 100 V.

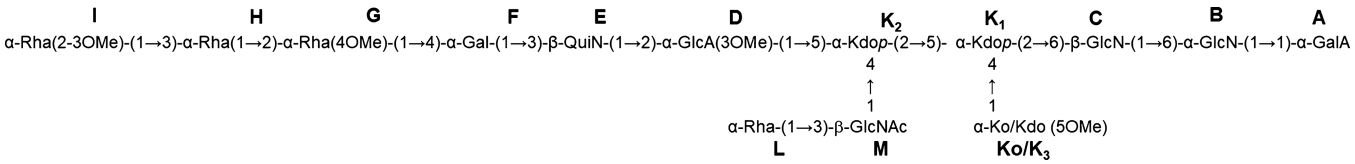

noting that the strong NOE contact observed between the anomeric protons of the *t*-α-GalA and α-GlcN as well as the corresponding long-range correlations were diagnostic for their trehalose-like α,α-(1 → 1) linkage occurring on the lipid A sugar backbone.

Ultrahigh-Resolution Mass Spectrometry of OS_{deAc}

The deacylated LOS sample ($\mathbf{OS_{deAc}}$) was also measured and structurally characterized by ultrahigh-resolution MS.[20] The structural elucidation was based on in-source fragmentation of the intact $\mathbf{OS_{deAc}}$ species and collision-induced dissociation (CID) of both intact and fragmented species, combined with the information from structural and compositional analyses (see Supporting Information text and figures). MS measurements in positive and negative-ion modes provided extensive information that allowed to confidently elucidate the structures. Two major OS species were identified, namely, $\mathbf{OS_{1deAc}}$ and $\mathbf{OS_{2deAc}}$. These were detected in positive mode ESI-MS at *m/z* 839.9755 (3+) and *m/z* 845.3073 (3+) and with mass measurement errors of 0.55 and 0.72 ppm, respectively (Figure 2). The mass difference between $\mathbf{OS_{1deAc}}$ and $\mathbf{OS_{2deAc}}$ was 15.9954 Da, which corresponded to an oxygen atom. Such a structural difference was localized and identified as the difference between a methylated Kdo residue ($C_9H_{14}O_7$, 234.0740 Da) and a methylated Ko residue ($C_9H_{14}O_8$, 250.0689 Da) present in the structure of $\mathbf{OS_{1deAc}}$ and $\mathbf{OS_{2deAc}}$, respectively. Ion species smaller than $\mathbf{OS_{1deAc}}$ and $\mathbf{OS_{2deAc}}$ showed mass differences corresponding to one or two methylene groups (i.e., 14.0157 Da or 28.0313 Da) or H_2O (i.e., 18.0106 Da). Larger ions were identified as sodium and potassium adducts.

The CID mass spectra of intact $\mathbf{OS_{1deAc}}$ and $\mathbf{OS_{2deAc}}$ are shown in Figure 2C,D, which indicated similarities between

https://doi.org/10.1021/jacsau.3c00025
JACS Au 2023, 3, 929−942

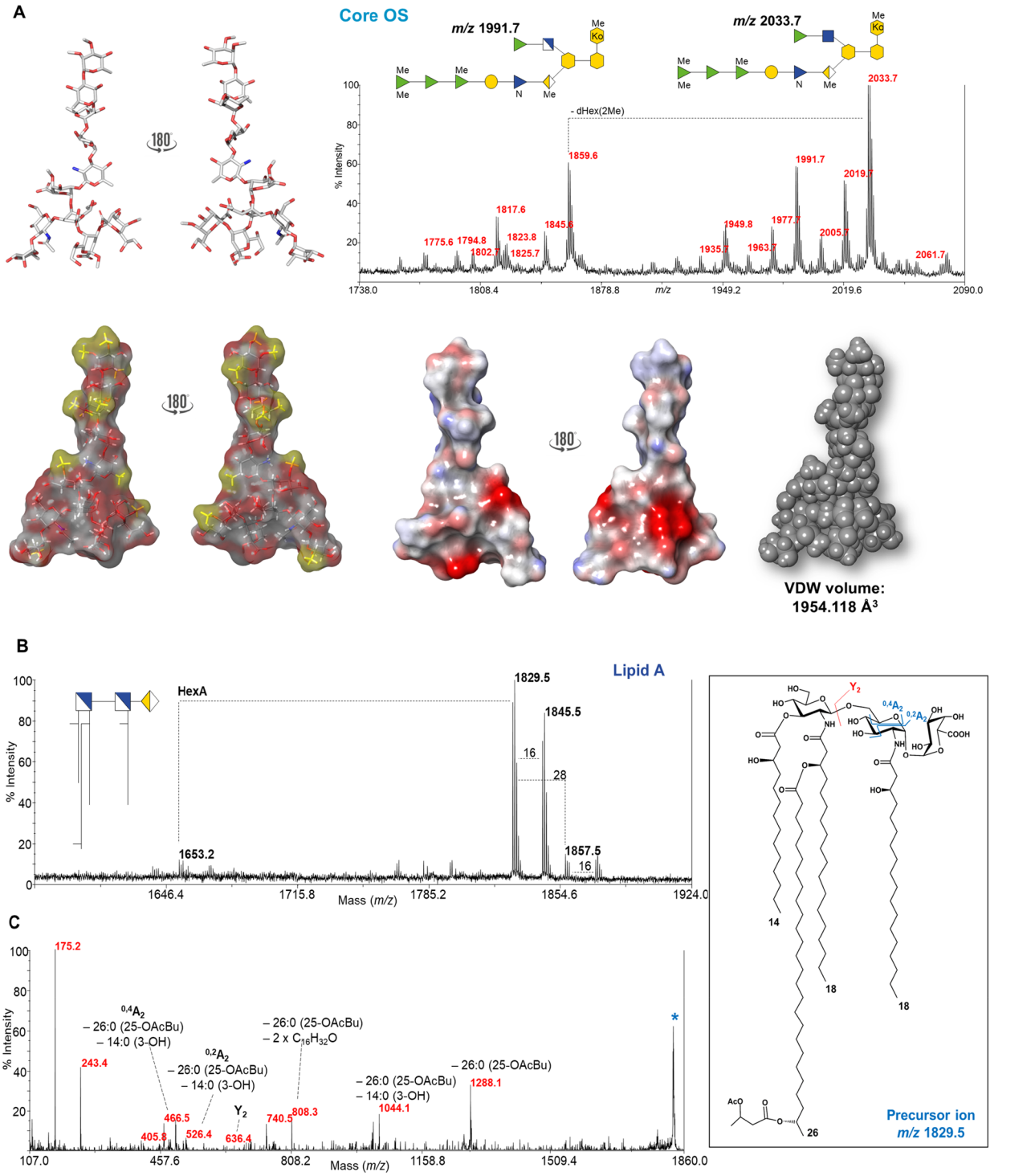

Figure 3. (A) Top panel: Negative-ion reflectron MALDI-TOF mass spectrum of a mild acid hydrolysis product of *M. extorquens* LOS. The proposed structures for the oligosaccharide species detected at *m/z* 1991.7 and *m/z* 2033.7 have been drawn by using Symbol Nomenclature for Glycans (SNFG). Symbols legend: green triangle: rhamnose; blue triangle with "N": quinovosamine; yellow/white diamond: galacturonic acid; blue square: *N*-acetyl-glucosamine; blue/white square: glucosamine yellow hexagon: 3-deoxy-D-*manno*-octulosonic acid, Kdo; yellow hexagon with "Ko": D-*glycero*-D-*talo*-2-octulosonic acid, Ko; Me: methylation. Bottom panel: Different views of the core OS 3D model. Either the VDW surface (on the left) or the molecular surface (on the right) is shown. Methyl groups have been depicted in yellow. The core OS 3D model with a molecular surface colored according to the interpolated charge as obtained by Discovery Studio Software (www.3dsbiovia.com). (B) Reflectron MALDI-TOF mass spectrum, recorded in negative polarity, of lipid A isolated from *M. extorquens*. Differences of 28 amu (a $-CH_2CH_2-$ unit) and 16 amu are also reported in the spectrum. HexA indicates hexuronic acid. (C) Negative-ion MALDI MS/MS spectrum of a precursor ion at *m/z* 1829.5 ascribed to a tetra-acylated lipid A species of LOS from *M. extorquens*. The assignment of main fragments is reported in the spectrum, and the proposed structure for the lipid A species is sketched in the inset. The peak originating from the loss of $C_{16}H_{32}O$ (240 mass units), because of a rearrangement occurring on amide-linked 3-OH acyl chains having the hydroxyl group free, has also been indicated. The asterisk indicates the precursor ion.

https://doi.org/10.1021/jacsau.3c00025
JACS Au 2023, 3, 929−942

the fragmentation patterns (e.g., $\mathbf{OS_{1deAc}}$ fragment at *m/z* 1545.5830 and $\mathbf{OS_{2deAc}}$ fragment at *m/z* 1545.5828). The mass difference of about 16 Da, ascribable to one oxygen atom, measured for certain CID fragment ions (as $\mathbf{OS_{2deAc}}$ fragment at *m/z* 492.1465 and $\mathbf{OS_{1deAc}}$ fragment at *m/z* 484.1490) and also for intact $\mathbf{OS_{1deAc}}$ and $\mathbf{OS_{2deAc}}$ species (see also Supporting Information) corresponded to the difference between a methylated Kdo residue ($C_9H_{14}O_7$, 234.0740 Da) and a methylated Ko residue ($C_9H_{14}O_8$, 250.0689 Da), alternatively present in $\mathbf{OS_{1deAc}}$ and $\mathbf{OS_{2deAc}}$, respectively. This structural difference, matching with NMR and compositional analysis, was therefore corroborated by the detailed evaluation of CID mass spectra of specific in-source fragment ions (Figures 2E,F and C,D, and Supporting Information). Furthermore, CID mass spectra also provided the distribution of Kdo and Ko residues in the inner core region; in particular, an internal Kdo/Ko trisaccharide initiated the core region, with a Kdo residue linked to the non-reducing GlcN of the lipid A backbone ($\mathbf{K_1}$, Figures 1A and 2) and branched by a terminal 5-*O*-methylated Ko/Kdo and a second Kdo, from which the core chain elongates (Figure 2C−E and Supporting Information).

Core OS Structure and Conformational Analysis

In parallel, the LOS underwent mild acid hydrolysis to split lipid A and the core oligosaccharide **OS**. A negative-ion MALDI-TOF MS analysis of **OS** (Figure 3A) further supported the abovementioned data and clearly showed the complex heterogeneity of the saccharide portion of *M. extorquens* LOS, mainly due to the non-stoichiometric *O*-methylation of different sugar units. It is worth noting that it was possible to observe an additional heterogeneity that consisted of the non-stoichiometric acetylation of the GlcN residue **E**. As shown in Figure 3A, the main **OS** species at *m/z* 2033.7 $[M - H]^-$ corresponded to an oligosaccharide made up of 4 dHex, 1 dHexN, 1 HexNAc, 1 HexA, 1 Hex, 1 Ko, 2 Kdo, and 5 methyl groups (Me), matching with $\mathbf{OS_{2deAc}}$**as** described above. Interestingly, an additional species was identified at *m/z* 1991.7 $[M - H]^-$ ($\Delta m/z$ = 42) and matched with a minor oligosaccharide carrying a non-acetylated HexN residue (Figure 3). Both peaks were flanked by peaks differing in 14 amu, clearly depicting the variability in the *O*-methylation pattern of **OS** (as also described above, Figure 2). Finally, minor species were detected at *m/z* 1859.6 $[M - H]^-$ and *m/z* 1817.6 $[M - H]^-$ differed by 174 amu and therefore lacked the bis-methylated terminal dHex unit.

The three-dimensional architecture of **OS** was described by computational approaches (Figure 3A). In detail, the disaccharide units contained in **OS** were constructed and the energetically accessible conformational regions were investigated by molecular mechanics (MM) calculations (see Supporting Information). The corresponding adiabatic energy maps for the glycosidic torsions Φ (H1−C1−O−CX′) and Ψ (C1−O−CX′−HX′; C1−O−CX′−CX′−1 for 6-linked sugars, Figure S5A) were used to build *M. extorquens* core **OS** and run MD simulation in explicit solvent with AMBER; it is worth highlighting that this was possible since we developed a parameter set for simulating the **OS** using the tools available in the AMBER suite of programs. Based on the results of the MD cluster analysis, the overall structural features of the model were investigated, and the saccharide conformation was estimated. The most representative conformers (Figures 3A and S5B) shared comparable shape and side chain patterns. The resulting computational model revealed the tendency of the **OS** to adopt a compact shape at the reducing end that forms a densely packed moiety stabilized by a network of polar contacts and hydrogen bonds, while the rest of the molecule adopted a stretched orientation protruding away from the bacterial surface. The extensive *O*-methylation along the saccharide chain decreased the hydrophilic character of core **OS** (Figure 3A), and a further reduction of number and distribution of hydroxyl groups was also ascribable to the presence of deoxy- and amino-sugars sugar chain. In addition, despite the absence of the canonical core-lipid A phosphate substituents, the presence of Kdo, Ko, and GalA residues defined a highly negatively charged and compact region in the inner core portion of **OS** (see Figures 2 and 3 and S5). These properties likely modulated the biophysical properties of *M. extorquens* LOS (and OM) and influenced interaction with and adaptation to the external environment (see below).

M. extorquens PA1 and *AM1* Lipid A Structural Characterization

Lipid A underwent compositional, NMR, and MS investigations. NMR analysis (Table S2 and Figure S6) showed a non-phosphorylated trisaccharide backbone [Glc*p*N-*β*-(1 → 6)-Glc*p*N-*α*-(1 → 1)-*α*-Gal*p*A] acylated at position 2 of the proximal GlcN and 2 and 3 of the distal GlcN. Only one VLCFA was evident from the NMR spectra, stoichiometrically esterified at the *ω*-1 position by a 3-*O*-acetyl-butyrate (OAcBu) residue (see below and Supporting Information text and figures). The negative-ion MALDI-TOF MS investigation of lipid A (Figure 3B) showed a heterogeneous pattern of signals in the *m/z*-range 1829.5−1873.5, ascribed to differently acylated non-phosphorylated tetra-acylated species; mass differences of 28 amu (−CH_2CH_2− unit) were diagnostic for different acyl chain lengths, while differences of 16 amu were attributed to further hydroxylation of acyl moieties (Figures 3B and S7). The main peak at *m/z* 1829.5 matched with a tetra-acylated lipid A species composed of a GlcN disaccharide backbone substituted by one hexuronic acid (HexA) and bearing two 18:0(3-OH), one 14:0(3-OH), and one VLCFA, that is, 26:0 (25-OAcBu). The exact location of acyl chains and of HexA on the GlcN disaccharide backbone was attained by a negative-ion MS/MS analysis (Figures 3 and S6). The MS/MS spectrum of a precursor ion at *m/z* 1829.5 (Figure 3c) showed an intense peak at *m/z* 1288.1 that was matched with an ion originated from the loss of 26:0 (25-OAcBu). The ion peak at *m/z* 1044.1 was attributed to the sequential loss of 26:0 (25-OAcBu) and 14:0 (3-OH), while the peak at *m/z* 808.3 was attributed to the loss of 26:0 (25-OAcBu) plus additional 480 amu, originated from an enamine to imine tautomerization, followed by a six-membered ring-based rearrangement, occurring only when the *N*-linked fatty acids have a free 3-OH group.[21] Since this rearrangement was only observed after the VLCFA was eliminated, it is plausible to hypothesize that the latter was in an acyloxyacyl amide moiety. Additional structural information was provided by the peak at *m/z* 466.5, originated from the sugar ring fragmentation ($^{0,4}A_2$)[22] plus the loss of VLCFA and 14:0(3-OH). The presence of this peak was fundamental to locate on the distal GlcN one 18:0(3-OH), one 14:0(3-OH), and one 26:0 (25-OAcBu) unit. This structural hypothesis was further supported by the detection of the peak at *m/z* 526.4 that was derived from the cross-ring fragmentations $^{0,2}A_2$ plus the loss of both 14:0(3-OH) and 26:0 (25-OAcBu). Therefore, the lipid

https://doi.org/10.1021/jacsau.3c00025
JACS Au 2023, 3, 929−942

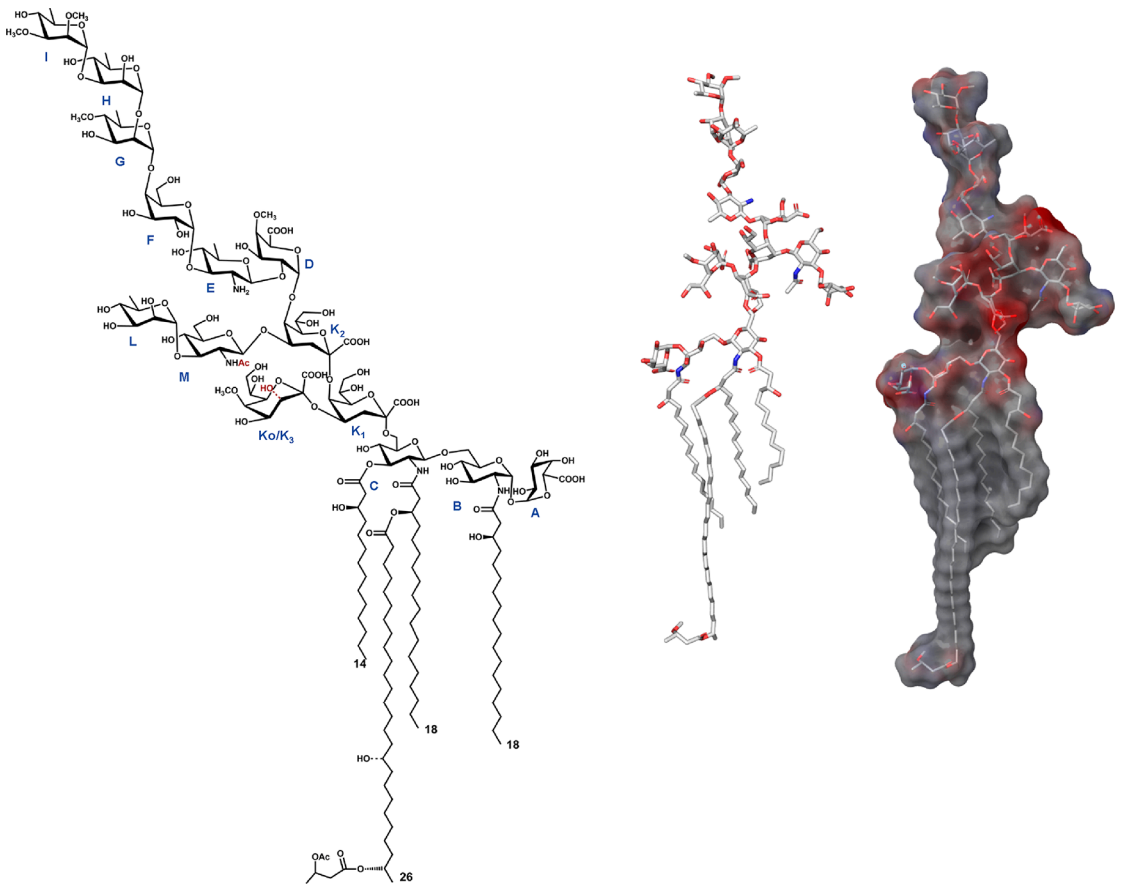

Figure 4. Full structure of *M. extorquens* PA1 and AM1 LOS. The LOS 3D model clearly showed the concentration of negative charges in the lipid A inner core region and illustrated the overall OS conformation characterized by a bent and densely packed moiety in its inner region and a more extended orientation at its terminal end.

A species detected at *m/z* 1829.5 was identified as a tetra-acylated structure carrying *N*-linked 18:0(3-OH) and *O*-linked 14:0(3-OH) as primary acyl chains on the distal GlcN and containing a 3-*O*-acetyl-butyryl-substituted VLCFA as a secondary acyl substituent of the 18:0(3-OH), while *N*-linked 18:0(3-OH) is the sole fatty acid occurring on the proximal GlcN residue, which in turn carries a GalA unit at its anomeric position. Finally, additional heterogeneity was found in the occurrence of lipid A species carrying on the VLCFA further hydroxylation (see Supporting Information and Figure S7).

M. extorquens PA1 and *AM1* LOS MALDI MS Analysis

An aliquot of intact LOS was analyzed by negative-ion MALDI-TOF MS. The MS spectrum (Figure S8) showed at higher molecular masses (3400−4300 *m/z*) a series of $[M - H]^-$ ions relative to the native LOS mixture, composed of species differing in the composition of both acyl and sugar moieties. Interestingly, ion fragments originated from the cleavage of the acid-labile glycosidic linkage between Kdo and the lipid A portion were also identified at lower mass ranges (*m/z* 1800−2500), which furnished important additional details about the structure of *M. extorquens* LOS. In particular, the extreme heterogeneity of the core OS region was noticeable; in particular, in the mass region 1991.7−2061.7, five main core OS species differing in the *O*-methylation degree were identified ($\mathbf{OS_A}$-$\mathbf{OS_E}$), whose proposed composition is sketched in the inset of Figure S8. Finally, the main LOS species matched with a combination of the various OS ion peaks and differently acylated lipid A species, thus giving rise to complex patterns of signals, clearly proving the high heterogeneity of such an LOS molecule (Figure S8). The full PA1 and AM1 LOS structure of *M. extorquens* PA1 and AM1 is depicted in Figure 4.

Morphological and Structural Characterization of *M. extorquens* LOS-Containing Lipid Bilayers

The external leaflet of bacterial OM also includes diacylphospholipids, with phosphoethanolamine and phosphoglycerol being the most abundant. Therefore, to study the effect of *M. extorquens* LOS on membrane properties, we prepared lipid bilayers composed by 1-Palmitoyl-2-oleoyl-*sn-glycerol*-3-phosphoethanolamine (POPE) and 1-palmitoyl-2-oleyl-*sn-glycerol*-3-phospho-(1′-*rac*-glycerol) (POPG) and investigated their morphological variation upon LOS inclusion (see details in the Methods section). This simplified model system was chosen in this explorative investigation to allow for an easier identification of the molecular determinants of the observed effects, which could be difficult to dissect in complex membranes. Extrapolation of the results to real biomembranes should be handled with care and would require further investigation of different, more realistic membrane models. Different complementary approaches were employed to analyze such membrane systems on different length scales. Preliminarily, SANS measurements were performed to compare the geometrical parameters of POPE/POPG and POPE/POPG/LOS vesicles, and qualitatively no significant differences in the scattering profile were detected. For both samples, the scattering intensity decreased with a q^{-2} power

https://doi.org/10.1021/jacsau.3c00025
JACS Au 2023, 3, 929−942

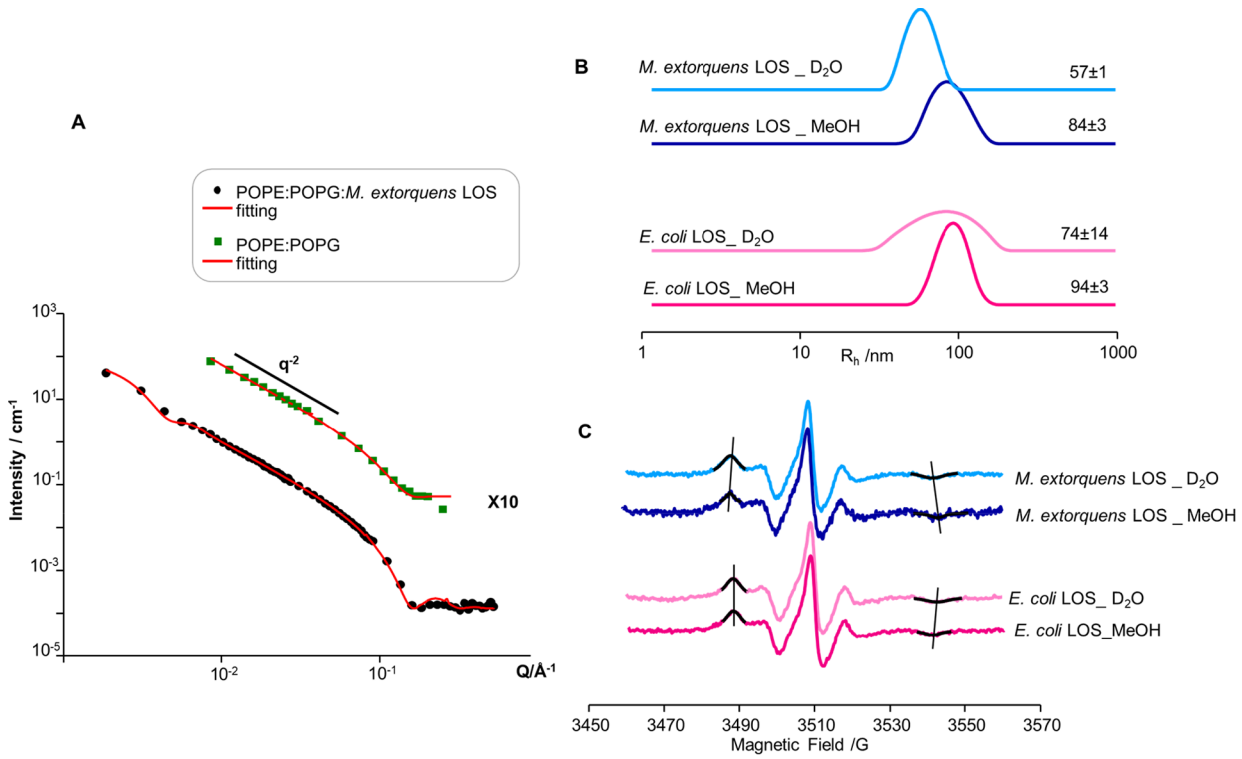

Figure 5. (A) SANS profiles and corresponding best-fitting curves of POPE/POPG (green squares) (acquired using a KWS-2 instrument located at Heinz Maier-Leibnitz Source, Garching Förschungszentrum, Germany[37]) and POPE/POPG/*M. extorquens* LOS (black circles) carried out using a D11 instrument located at Institut Laue Langevin, Grenoble, France. (B) Hydrodynamic radius distribution and (C) EPR spectra of 5-PCSL in POPE/POPG/*M.extorquens* LOS (49/21/30 molar ratio) and POPE/POPG/*E. coli* LOS (49/21/30 molar ratio) vesicles in D_2O (light blue and light pink lines, respectively) and in D_2O/MeOH mixtures (9%vol methanol, blue and pink lines, respectively).

law, suggesting that the insertion of LOS into the POPE/POPG mixture did not alter the tendency of the latter to form unilamellar vesicles (Figure 5A). However, according to the structural parameters obtained by the fitting procedure and shown in Table S3, the size and the bilayer thickness of the POPE/POPG vesicles increased upon insertion of *M. extorquens* LOS.

With the aim to analyze whether *M. extorquens* LOS affected the membrane response to the presence of methanol in the aqueous medium, we performed DLS and EPR investigation of POPE/POPG/LOS vesicles in D_2O and in a mixture of D_2O/MeOH (9% v/v) (Figure 5B,C). In order to discern the specific effects of *Methylobacterium* LOS on the OM, lipid bilayers including *E. coli* LOS were also considered as a comparison. The distributions of the hydrodynamic radius R_h, reported in Figure 5B, revealed the presence of a single vesicle population in all cases. However, some differences were observed in terms of vesicle size. The presence of *M. extorquens* LOS causes the formation of smaller vesicles than those formed with *E. coli* LOS in both solvent systems. The presence of methanol caused an R_h increase, the variation being higher for samples including *M. extorquens* LOS than for those with *E. coli* LOS.

To better understand the effect of the environment on the lipid organization within the bilayers, EPR measurements were performed using the 5-PCSL spin-label, thus allowing for a direct detection of the lipid ordering and dynamics. The outer hyperfine splitting, $2A_{max}$, which is the distance between the first maximum and the second minimum, expressed in G, is determined by the amplitude and the rate of lipid tail rotational motion and is a well-recognized index of the acyl chain dynamics and ordering.[23] Figure 5C shows that $2A_{max}$ increases in the presence of methanol for bilayers including *M. extorquens* LOS. In contrast, lipid bilayers including *E. coli* LOS showed an opposite behavior (see also Table S4). This evidence points to a peculiar ability of *M. extorquens* LOS to induce a bilayer ordering in the presence of methanol.

DISCUSSION

M. extorquens, in particular strain AM1, has been the most extensively studied methylotroph for over 50 years[24] as a promising candidate for the bioproduction of value-added compounds from methanol.[8] This remarkable property represents a crucial distinctive feature, in a period of accretive industrialization and growing world population, when the use of alternative carbon sources is not only encouraged but steadily becoming mandatory. Notably, the intrinsic toxicity of methanol can be considered an additional advantage, as most microorganisms are unable to grow on it and hence contaminate fermentation processes, ensuring the bioproduction of high-quality compounds.

M. extorquens occupies ecologically diverse habitats which, together with the methylotrophic property, raises questions about the structure and flexibility of the bacterial cell surface membrane and its constituents, for handling a variety of possible biotic and abiotic stresses that this microorganism can encounter. Previous studies showed that *M. extorquens* possesses a very simple lipidome, with only 25 phospholipid species identified.[25] However, it also possesses most of the lipid structural features found in more complex organisms, including poly-unsaturated fatty acids, phosphatidylcholine, hopanoids, and carotenoids. The combination of a simple but

https://doi.org/10.1021/jacsau.3c00025
JACS Au 2023, 3, 929−942

distinctive lipidome has been proposed to serve complementary roles in OM adaptation.[26] In this frame, a significant part of *M. extorquens* lipidome is occupied by the lipid A portion of the LOS (Figure 4), which is the main constituent of the OM, constantly exposed to highly mutable environmental stimuli and dangers.

From a strict LPS chemistry point of view, here, we showed that *M. extorquens* lipid A has a non-phosphorylated tetra-acylated sugar skeleton, carrying 18:0(3-OH) and 14:0(3-OH) as primary acyl chains on the distal GlcN, and a secondary 26:0(25-OH) [minor 28:0(27-OH)], in turn acylated by a novel 3-*O*-acetyl-butyrate residue, which to the best of our knowledge has never been found in lipid A. It is worth noting that the proximal GlcN was exclusively substituted by an *N*-linked 18:0(3-OH) and carried a GalA unit at its anomeric position (Figure 4) through a trehalose-type linkage α,α-(1 → 1). Therefore, *M. extorquens* AM1 and PA1 lipid A show an asymmetric 3 + 1 distribution of the acyl chains with respect to the GlcN backbone, with the proximal GlcN carrying a single acyl moiety, and (ω-1) hydroxylated VLCFAs, synthesized by a very limited group of bacteria, besides rhizobia.[27−30] Notably, the saccharide backbone is also worth commenting on, as whether non-phosphorylated backbones have been previously described for lipid A of environmental and plant-associated strains,[14,31] here the lack of substituents at position 4 of the non-reducing GlcN (usually phosphorylated or glycosylated) is certainly remarkable. Likewise the replacement of the phosphate on the proximal GlcN with GalA has been already detected in lipid A deriving from other bacterial species such as those belonging to the *Rhopseudomonas* genus, namely, *R. palustris*[21] and *R. viridis*,[32] as well as Rhizobiaceae (i.e., *Brady-*, *Azo-*, and *Mesorhizobium* genera)[27,28,33,34] and *Oligotropha carboxidovorans*,[29] which, however, are characterized by the occurrence of GalA connected to a reducing 2,3-diamino-2,3-dideoxy-glucose. On the other hand, lipid A from *Acetobacter pasteurianus*, a plant-associated bacterium able to produce acetic acid, has a proximal GlcN that instead carries a glucuronic acid at its anomeric position.[35] Ko has been so far found in a few bacterial species, like *Burkholderia* and *Acinetobacter*, never *O*-methylated. The *O*-methylation of LOS *O*-antigen residues, Rhamnose included, is instead more frequently found in plant-associated bacteria, either Exopolysaccharides or Lipopolysaccahrides.[14,38,39]

As for the core OS, this was characterized by an extensive, multiple non-stochiometric *O*-methylation of the sugar residues, distributed along the whole saccharide chain. This included the novel and unprecedented *O*-methylation at position O5 on the alternative terminal Kdo/Ko units and the extreme non-reducing core region that was capped by a rhamno-trisaccharide chain extensively *O*-methylated, which further decreases the hydrophilicity of the outermost portion of the LOS (Figure 4). Furthermore, in the lipid A inner core region, a series of negatively charged sugar units (Kdo, Ko, and GalA) created a region with a high negative electrostatic potential (Figure 3), partially mitigated by the two aminosugar residues. In the presence of divalent ions, such as calcium ions, which are commonly present in biological media and are able to act as crosslinking agents, such a high concentration of negative charges increases the stability of the OM through the establishment of a thick network of electrostatic interactions, while the outer core region protruded away from the bacterial surface.

These features, charge distribution and low hydrophilicity of the outer core region, were further investigated by MD simulation and biophysical analyses. Computational data defined the overall shape of the core OS, which assumed a narrow shape in the inner region and a more extended disposition at its terminal end. In addition, the hydrophilic sugar backbone was amply scaled down by methyl groups. It is worth noting that this vast and spread methylation could be deemed an option to modulate the glycans chemical structure and biophysical properties, facilitate the molecular dialogue with the host, mediate symbiotic and environmental interactions,[36] and constitute a conserved target of the host innate immune system.[37,38] In this frame, we have already demonstrated the ability of *M. extorquens* PA1 to produce exopolysaccharide mixtures[39] altered if grown in the presence of methanol and with a variable degree of methylation that influenced the 3D structure, supramolecular assets, diffusion properties, and hydrodynamic radius, thus contributing to increased methanol tolerance and cell stability.

As for the supramolecular properties of the OM, the abovementioned structural peculiarities impact the response of the membrane to the presence of methanol, in terms of fluidity, as shown by our biophysical investigation on phospholipid bilayers. Methanol is reported to have a destructuring effect on phospholipid membranes, due to an increased disorder of the acyl chains.[40−42] The number of hydrogen bonds formed between methanol and lipid heads is low since it remains mainly hydrated by water.[43] However, because of the hydrophobicity of the methyl groups, methanol partially penetrates the membrane, although just below the head-group region, because of the bulk and polarity of the hydrated part. The accumulation of methanol molecules in this region disrupts lipid packing, eventually leading to membrane disruption. We also observed the destructuring effect of methanol on lipid bilayers, including those with *E. coli* LOS, but we demonstrated that *M. extorquens* LOS stabilizes the bilayer once in the presence of methanol, increasing the lipid ordering, and reducing the membrane fluidity. This is a unique behavior, never been described before.

The unambiguous identification of the molecular features responsible for the peculiar behavior of the bilayers including *M. extorquens* LOS in the presence of methanol is a difficult task. Certainly, as a whole, the peculiar structure of the core OS is likely to play a key role. Rhamnose exhibits low compatibility with water, as confirmed by the extremely low hydration number.[44] This solvophobicity is enhanced by the presence of methanol.[45] As a result, Rha residues located at the termini of the outer core region and protruded from the bacterial surface tend to form a compact layer, shielding the underlying membrane regions from exposure to the external aqueous medium. The extensive methylation further enhances this protective action. The strengthening of the intermolecular interactions between the core OS residues in the presence of methanol leads to an observed reduction of the membrane curvature (an increase of hydrodynamic radius). Finally, the limited number of acyl chains of lipid A allows them to easily adapt to changes in the curvature/mesostructure of the membrane, whose integrity is strengthened by the VLFA, with the result of an increase in the acyl chain ordering.

In conclusion, it is possible to assert that the structure of *M. extorquens* LOS is well suited to induce ordering and strengthening of the asymmetric OM and support bacterial survival, allowing them to live in the presence of methanol and

https://doi.org/10.1021/jacsau.3c00025
JACS Au 2023, 3, 929−942

use it, thus enabling various biotechnical applications for this resource in the future.

METHODS

Bacteria Isolation and Growth

Methylobacter extorquens AM1 cells were grown in 10 liters of succinate methanol medium [30 mM succinate, 150 mM MeOH, 30 mM NH_4Cl, 0.81 mM $MgSO_4$, 40 μM Na_2-EDTA, 11 μM $FeSO_4$, 16 μM $ZnSO_4$, 13 μM $CoCl_2$, 5 μM $MnCl_2$, 16 μM H_3BO_3, 1.65 μM Na_2MoO_4, 1.2 μM $CuSO_4$, 20.4 μM $CaCl_2$, 10 mM phosphate buffer (pH 6.7)] at 28 °C and shaken at 150 rpm up to reach the end of the growth curve's exponential phase (4 days after inoculation). The cells were collected by centrifugation at 4000 g for 30 min, and the pellets were lyophilized to produce approximatively 8 g of dried cells.

Isolation and Purification of LOS from *M. extorquens* PA1 and AM-1

Dried bacterial cells were extracted following the petroleum ether/chloroform/phenol procedure. To define the nature of the extracted material, an SDS-PAGE followed by silver nitrate gel staining was performed, revealing the rough nature of the LPS isolated from both strains. To remove proteins and nucleic acids, an enzymatic digestion with RNase (Sigma-Aldrich, Darmstadt, Germany), DNase (Sigma-Aldrich, Darmstadt, Germany), and Proteases (Sigma-Aldrich, Darmstadt, Germany) (37 and 56 °C) was performed. In addition, an ultracentrifugation step (4 °C, 100,000*g*, 16 h) and a size-exclusion chromatography on a Sephadex-75 column were executed.

Chemical Analyses

The monosaccharide content of both LOS was determined by analysis of the acetylated *O*-methyl glycoside derivatives obtained by a treatment with HCl/MeOH (1.25 M, 85 °C), followed by an acetylation step with acetic anhydride in pyridine (85 °C, 30 min). The absolute configuration was defined as previously described through the analysis of the *O*-octylglycoside derivatives.[46] To determine the sugar linkage pattern, an aliquot of each LOS was suspended in dimethyl sulfoxide in the presence of NaOH, alternating stirring and sonication for 2 h at room temperature, and then it was methylated with CH_3I, hydrolyzed with trifluoroacetic acid (4 M, 100 °C, 4 h), carbonyl-reduced with NaBD4, and acetylated. The total fatty acid content was determined on intact LOSs and on isolated lipid A fractions by treating with HCl (4 M, 100 °C, 4 h), followed by NaOH (5 M, 100 °C, 30 min). The pH was adjusted to 3. An extraction in chloroform allowed us to isolate the fatty acids that were then methylated with diazomethane. All chemical analyses were performed by means of gas−liquid chromatography Agilent Technologies 6850A (Santa Clara, CA, USA) equipped with a mass selective detector 5973 N and a Zebron ZB-5 capillary column (Phenomenex, 30 m × 0.25 mm i.d., 0.25 μm as film thickness, flow rate 1 mL/min, He as carrier gas). The temperature program (140 °C for 5 min, 140 °C → 280 °C at 10 °C/min, and 280 °C for 10 min) was used for lipid analysis, whereas for sugar analysis, the temperature program was 150 °C for 5 min, 150 °C → 280 °C at 3 °C/min, and 280 °C for 5 min.

Isolation of the OS_{deAc} Fraction

In order to define the structure of the core OS of LOS *M. extorquens* PA1 and AM-1, a 40 mg aliquot of both LOS underwent a *O*-deacylation with anhydrous hydrazine (2 mL, at 37 °C for 90 min), and then it was cooled, poured into ice-cold acetone, and allowed to precipitate. The precipitate was then centrifuged (5000×*g*, 30 min), washed with ice-cold acetone, dried, dissolved in water, and lyophilized. The *O*-deacylated product was then *N*-deacylated with 4 M KOH (120 °C, 16 h). The removal of salts was performed by gel-filtration chromatography on a Sephadex G-10 column (Pharmacia, 50 × 1.5 cm).

Isolation of the OS and Lipid a Fractions

An aliquot (5 mg) of each LOS was also treated with acetic acid at 100 °C for 4 h to allow for the separation between the lipid A and the core OS portion. The solutions were extracted three times with $CHCl_3$/MeOH/H_20 (100:30:30, v/v/v) and centrifuged (4 °C, 7000×*g*, 15 min). The organic phases containing the lipid A were then further purified by three washes with distilled water and then freeze-dried. The water-soluble fraction was also collected and lyophilized.

NMR Spectroscopy

For structural assignments of isolated polysaccharides NMR spectra were recorded in D_2O at 298 K at pD 7 with a cryoprobe-equipped Bruker 600 MHz AVANCE NEO. TOCSY experiments were performed with spinlock times of 100 ms using data sets (t1 × t2) of 4096 × 512 points. Rotating-frame Overhauser enhancement spectroscopy and nuclear Overhauser enhancement spectroscopy experiments were performed using data sets (t1 × t2) of 4096 × 512 points with mixing times between 100 and 400 ms. Double-quantum-filtered phase-sensitive correlation spectroscopy (DQF-COSY) experiments were performed using data sets of 4096 × 912 points. The data matrix in all homonuclear experiments was zero-filled in both dimensions to give a matrix of 4 K × 2 K points and was resolution-enhanced in both dimensions using a cosinebell function before Fourier transformation. Coupling constants were determined by 2D phase-sensitive DQF-COSY measurements. HSQC and HMBC experiments were performed in the ^{1}H-detection mode by single-quantum coherence with proton decoupling in the ^{13}C domain using data sets of 2048 × 400 points. HSQC was performed using sensitivity improvement and in the phase-sensitive mode using echo/antiecho gradient selection, with multiplicity editing during the selection step. HMBC was optimized on long-range coupling constants, with a low-pass J filter to suppress one-bond correlations, using gradient pulses for selection. Moreover, a 60 ms delay was used for the evolution of long-range correlations. HMBC spectra were optimized for 6−15 Hz coupling constants. The data matrix in all the heteronuclear experiments was extended to 2048 × 1024 points by using a forward linear prediction extrapolation.

Ultrahigh-Resolution Mass Spectrometry

Dried deacylated LOS ($\mathbf{OS_{deAc}}$) was reconstituted with 100 μL of water. Then, 4 μL of $\mathbf{OS_{deAc}}$ solution was diluted with 196 μL of a 50:50 (v/v) ACN:water solution. Direct infusion ESI FT-ICR MS measurements were performed on a 15 T solariX XR FT-ICR MS system (Bruker Daltonics) equipped with a Combi-Source and a ParaCell, at a flow rate of 2 μL/min with a capillary voltage of 4500 V. Mass spectra were acquired in positive and negative-ion modes in the *m/z*-range 92−5000 with 2 M data points. In-source CID analysis was performed by increasing the skimmer voltage (from 15 V up to 100 V). MS/MS analysis of selected precursor ions was performed by CID, in the collision hexapole cell, with optimized isolation windows, collision energies, and accumulation time. The ESI mass spectra were obtained from the sum of a different number of scans. For MALDI analysis, 1 μL of the reconstituted $\mathbf{OS_{deAc}}$ was diluted with 9 μL of water. Then, 1 μL of this solution was spotted onto a ground-steel MALDI target plate with 1 μL of a 10 mg/mL solution of "super-2,5-dihydroxybenzoic acid (DHB)" [a 9:1 (w/w) mixture of DHB and 2-hydroxy-5-methoxybenzoic acid] in a 50:50 ACN:water (v:v) solution. MALDI-CID FT-ICR MS measurements were performed in positive ion mode in the *m/z*-range 298.8−5000 with 1 M data points.[20]

Data Analysis

The mass spectra were visualized in DataAnalysis 5.0 SR1 (Bruker Daltonics) software, and mass differences between the detected fragment ions were evaluated. Theoretical *m/z*-values of the fragment ions were generated in GlycoWorkbench 2[47,48] and matched with the acquired data.

MALDI-TOF Mass Spectrometry

Linear and Reflectron MALDI-TOF MS spectra of lipid A, intact LOS, and its related mild acid hydrolysis product (**OS**) were recorded on an ABSCIEX TOF/TOF 5800 Applied Biosystems mass spectrometer equipped with an Nd:YAG laser (λ = 349 nm), with a 3-ns pulse width and a repetition rate of up to 1000 Hz. Lipid A

https://doi.org/10.1021/jacsau.3c00025
JACS Au 2023, 3, 929−942

fraction was dissolved in $CHCl_3/CH_3OH$ (1:1, v/v). The matrix solution was 2,4,6-trihydroxyacetophenone (THAP) in CH_3OH/0.1% TFA/AcN (7:2:1, v/v) at a concentration of 75 mg/mL. As for the intact LOS, 1 mg/mL solution in distilled water was prepared and then mixed with DHB, which was suspended in 0.1% citric acid.[49] Finally, the mild acid hydrolysis product dissolved in distilled water was mixed with THAP in acetonitrile with 0.1% TFA (1:1). Each spectrum in the MS experiments was a result of the accumulation of 2000 laser shots, whereas 5000−7000 shots were summed for the MS/MS spectra. Each experiment was performed in duplicate.

Preparation of Biomembrane-Mimicking Lipid Bilayers

POPE and POPG were purchased from Avanti Polar Lipids (Birmingham, AL, USA, purity >99%), and their solutions were prepared at a POPE/POPG 70/30 molar ratio in chloroform. LOS was also dissolved in chloroform. Samples were prepared by mixing suitable volumes of POPE/POPG solution with an appropriate volume of LOS solution to get a 70/30 phospholipids/LOS molar ratio. For EPR spectroscopy, an aliquot of a spin-labeled phosphatidylcholine (5-PCSL, Sigma-Aldrich, Milan, Italy, purity >99%) in ethanol solution was added at 2% by weight on total lipids. A thin film of lipids was obtained through evaporation of the solvent with dry nitrogen gas and vacuum desiccation. Then, D_2O and D_2O/MeOH (9%vol) mixtures were alternatively added to dry lipid films to yield a total lipid concentration of 1 mg/mL. For the SANS measurements, only D_2O was used as solvent. Samples were then repeatedly vortexed to obtain multilamellar vesicle suspensions, which were used as such for EPR experiments. For SANS and DLS experiments, these suspensions were extruded through polycarbonate membranes of 100 nm pore size for 25 times to obtain unilamellar vesicle suspensions.

Small-Angle Neutron Scattering

SANS measurements were performed on D11 at the Institut Laue Langevin (ILL), Grenoble (France). Neutrons with a wavelength spread $\Delta\lambda/\lambda \leq 0.09$ were used. A two-dimensional array detector at three different wavelengths (W)/collimation (C)/sample-to-detector (D)/distance combinations were used to measure neutrons scattered from the samples. These configurations allowed collecting data in a range of the scattering vector modulus $q = 4\pi/\lambda\sin(\theta/2)$ between 0.008 and 0.5 $Å^{-1}$. The investigated systems were contained in a closed quartz cell to prevent solvent evaporation. The raw data were then corrected for background and empty cell scattering. The obtained scattering intensity data, $I(q)$, were plotted as a function of q. Generally, the dependence of $I(q)$ from the scattering vector can be summarized as in eq 1

$$I(q) = \phi_P V_P P(q) S(q) + bkg \tag{1}$$

where ϕ_P, V_P, $P(q)$, and $S(q)$ represent the volume fraction of the particles, the particle volume, and the form and the structure factor of the scattering particles, respectively, while bkg is the incoherent and inelastic part of the scattered cross-section, largely dependent on any hydrogen present. The form factor accounts for the shape, size, and size distribution of the scattering particles, while a contribution of the structure factor can be considered when an interparticle correlation exists. The structural information contained in both the form and the structure factor can be extrapolated by choosing an appropriate model to fit the experimental data. In this case, the vesicle model was used to fit the data, utilizing the SasView software (version 5.0). Using this model, the 1D scattering intensity is calculated in the following way

$$P(q) = \frac{\phi}{V_{shell}} \times \left[\frac{3V_{core}(\rho_{solvent} - \rho_{shell}) j_1(qR_{core})}{qR_{core}} + \frac{3V_{tot}(\rho_{shell} - \rho_{solvent}) j_1(qR_{tot})}{qR_{tot}} \right]^2 + bkg \tag{2}$$

where ϕ is the volume fraction of the shell, V_{shell} is the volume of the shell, V_{core} is the volume of the core, V_{tot} is the total volume, R_{core} is the radius of the core, R_{tot} is the outer radius of the shell, $\rho_{solvent}$ is the scattering length density of the solvent, ρ_{shell} is the scattering length density of the bilayer, and j_1 is the spherical Bessel function. The fit data were given in terms of radius = R_{core} and thickness = $R_{tot} - R_{core}$. These data were compared with the POPE/POPG vesicle, which were acquired using the KWS-2 instrument located at Heinz Maier-Leibnitz Source, Garching Förschungszentrum, Germany, and reported in our previous work.[50]

Dynamic Light Scattering

DLS measurements were performed with a home-made instrument composed of a Photocor compact goniometer, a SMD 6000 Laser Quantum 50 mW light source operating at 532.15 nm, a photomultiplier (PMT-120-OP/B), and a correlator (Flex02-01D) from Correlator.com. The experiments were carried out at a constant temperature (25.0 ± 0.1)°C, by using a thermostatic bath, and at the scattering angle θ of 90°. The hydrodynamic radius R_h was determined from the diffusion coefficient of scattered particles D. In the approximation of spherical objects, continuous medium, and infinite dilution, D can be related to the R_h through the Stokes−Einstein equation

$$R_h = \frac{k_B T}{6\pi\eta D} \tag{3}$$

where k_B is the Boltzmann constant, T is the absolute temperature, and η is the solvent viscosity.

EPR Spectroscopy

EPR spectra of 5-PCSL in multilamellar vesicles were recorded on a 9 GHz Bruker Elexys E-500 spectrometer (Bruker, Rheinstetten, Germany). Spin-labeled samples were transferred in capillaries and flame-sealed. Capillaries were coaxially allocated in a standard quartz tube (4 mm i.d.) within the resonance cavity. The spectra were recorded at 25 °C by using the following acquisition parameters: sweep width, 120 G; resolution, 1024; time constant, 10.24 ms; modulation frequency, 100 kHz; modulation amplitude, 1.0 G; incident power, 6.33 mW. To improve the signal-to-noise ratio, 64 scans were accumulated.

MM and MD Simulation

The adiabatic maps of OS constituting disaccharides were constructed by using Maestro package (www.schrodinger.com/). In detail, MM calculations were performed with the MM3* forcefield as included in MacroModel 8.0. A di-electric constant of 80 was used. Extended nonbonded cut-off distances (a van der Waals cut-off of 8.0% and an electrostatic cut-off of 20.0%) were used. For each disaccharide structure, both Φ and Ψ were varied incrementally with use of a grid step of 18°, each (Φ,Ψ) point of the map being optimized with 2000 P.R. conjugate gradients. MD simulations were carried out using AMBER 18 suite of programs.[51] Parameters for non-standard residues, that is, Kdo, Ko, and QuiN, which are not included in the GLYCAM-web site, were generated by following a home-made protocol (manuscript in preparation) and used as building blocks to construct the OS. Atom types and charges were assigned according to AMBER GLYCAM-06j-1 force field. By using the Leap module, the ligands were hydrated with octahedral boxes containing explicit TIP3P water molecules 10 Å away from any atom; also, counter ions were added to neutralize the system. The systems minimization was performed using Sander, and MD simulations were carried out using the CUDA, which are distributed within the AMBER 18 package. The SHAKE algorithm was applied to all hydrogen containing bonds, and a 2 fs integration step was used. Long-range electrostatic interactions were computed by using periodic boundaries along with particle-mesh Ewald summation. Isothermal and isobaric conditions were used along the simulation. Temperature was maintained at 300 K with the Langevin thermostat applying a collision frequency of 1.0 ps^{-1} while pressure was kept at 1.0 atm. Energy minimization of the solvated systems was performed with solute restraints that were decreasing gradually from 100 kcal/mol with no restraints. Temperature was increased from 0 to 100 K at constant volume and then from 100 to 300 K in an isobaric ensemble. Thereafter, the temperature was kept

https://doi.org/10.1021/jacsau.3c00025
JACS Au 2023, 3, 929−942

constant at 300 K during 50 ps with progressive energy minimizations and a solute restraint. Once completed, the restraints were removed and the systems were then advanced in an isothermal-isobaric ensemble along the production. Trajectory coordinates were sampled every ps in order to acquire 10,000 structures of the progression of the dynamics. Trajectories were visualized with VMD molecular visualization program[52] and analyzed with the ptraj module included in the AMBER18. Pymol 2.3 Software (https://pymol. org/2/) and Discovery Studio Software were used to visualize and draw the molecules.

■ ASSOCIATED CONTENT

Supporting Information

The Supporting Information is available free of charge at https://pubs.acs.org/doi/10.1021/jacsau.3c00025.

NMR, MS, and MS/MS spectra of core OS and lipid A, full MS structural discussion of core OS and related MS and MS/MS spectra, and full NMR structural description of lipid A (PDF)

■ AUTHOR INFORMATION

Corresponding Author

Alba Silipo − *Department of Chemical Sciences and Task Force for Microbiome Studies, University of Naples Federico II, 80126 Naples, Italy;* orcid.org/0000-0002-5394-6532; Email: silipo@unina.it

Authors

Flaviana Di Lorenzo − *Department of Chemical Sciences and Task Force for Microbiome Studies, University of Naples Federico II, 80126 Naples, Italy*

Simone Nicolardi − *Center for Proteomics and Metabolomics, Leiden University Medical Center, Leiden 2333 ZA, The Netherlands;* orcid.org/0000-0001-8393-1625

Roberta Marchetti − *Department of Chemical Sciences and Task Force for Microbiome Studies, University of Naples Federico II, 80126 Naples, Italy;* orcid.org/0000-0002-7173-7099

Adele Vanacore − *Department of Chemical Sciences and Task Force for Microbiome Studies, University of Naples Federico II, 80126 Naples, Italy*

Noemi Gallucci − *Department of Chemical Sciences and Task Force for Microbiome Studies, University of Naples Federico II, 80126 Naples, Italy; CSGI, Consorzio Interuniversitario per lo Sviluppo dei Sistemi a Grande Interfase, Florence 50019, Italy*

Katarzyna Duda − *Research Center Borstel Leibniz Lung Center, 23845 Borstel, Germany*

Ferran Nieto Fabregat − *Department of Chemical Sciences and Task Force for Microbiome Studies, University of Naples Federico II, 80126 Naples, Italy;* orcid.org/0000-0001-9847-3030

Ha Ngoc Anh Nguyen − *B-CUBE Center for Molecular Bioengineering, Technische Universität Dresden, 01307 Dresden, Germany*

Djamel Gully − *IRD, Laboratoire des Symbioses Tropicales et Méditerranéennes (LSTM) UMR IRD/SupAgro/INRA/UM2/CIRAD, 34398 Montpellier Cedex 5, France*

James Saenz − *B-CUBE Center for Molecular Bioengineering, Technische Universität Dresden, 01307 Dresden, Germany*

Eric Giraud − *IRD, Laboratoire des Symbioses Tropicales et Méditerranéennes (LSTM) UMR IRD/SupAgro/INRA/UM2/CIRAD, 34398 Montpellier Cedex 5, France*

Luigi Paduano − *Department of Chemical Sciences and Task Force for Microbiome Studies, University of Naples Federico II, 80126 Naples, Italy; CSGI, Consorzio Interuniversitario per lo Sviluppo dei Sistemi a Grande Interfase, Florence 50019, Italy*

Antonio Molinaro − *Department of Chemical Sciences and Task Force for Microbiome Studies, University of Naples Federico II, 80126 Naples, Italy;* orcid.org/0000-0002-3456-7369

Gerardino D'Errico − *Department of Chemical Sciences and Task Force for Microbiome Studies, University of Naples Federico II, 80126 Naples, Italy; CSGI, Consorzio Interuniversitario per lo Sviluppo dei Sistemi a Grande Interfase, Florence 50019, Italy;* orcid.org/0000-0001-6383-8618

Complete contact information is available at: https://pubs.acs.org/10.1021/jacsau.3c00025

Author Contributions

[¶]F.D.L. and S.N. contributed equally to this work. A.S. conceived the study and designed the research. S.N. carried out MS analysis of deacylated LOS. F.D.L. carried out the MS analysis of LOS, Core and Lipid A. R.M. carried out the parametrization of the OS and the computational studies. A.V. extracted, purified, and analyzed the data. N.G., L.P., and G.D. performed scattering and EPR experiments. All the authors contributed to analyzing the data and writing the manuscript and have given approval to the final version of the manuscript. CRediT: **Flaviana Di Lorenzo** data curation, formal analysis, investigation, methodology, writing-original draft, writing-review & editing; **Simone Nicolardi** data curation, formal analysis, investigation, methodology, writing-original draft, writing-review & editing; **Roberta Marchetti** data curation, investigation, methodology, writing-original draft, writing-review & editing; **Adele Vanacore** formal analysis, investigation; **Noemi Gallucci** formal analysis, investigation; **Katarzyna A. Duda** investigation; **Ferran Nieto Fabregat** investigation; **Ha Ngoc Anh Nguyen** investigation; **Djamel GULLY** investigation; **James P. Saenz** investigation; **Eric Giraud** investigation; **Luigi Paduano** investigation, writing-original draft, writing-review & editing; **Antonio Molinaro** investigation, writing-original draft, writing-review & editing; **Gerardino D'Errico** investigation, writing-original draft, writing-review & editing; **Alba Silipo** conceptualization, data curation, funding acquisition, investigation, project administration, supervision, validation, visualization, writing-original draft, writing-review & editing.

Notes

The authors declare no competing financial interest.

■ ACKNOWLEDGMENTS

A.S. was supported by PRIN 2017 (2017XZ2ZBK, 2019-2023); R.M. was supported by the European Research Council (ERC) under the European Union's Horizon 2020 research and innovation program under grant agreement No 851356; F.D.L. was supported by the ERC under the Horizon Europe program under grant agreement No. 101039841 (DEBUGGING LPS); and J.S. was supported by a German Federal Ministry of Education and Research BMBF grant (project 03Z22EN12) and a VW Foundation "Life" grant (project 93090). European Union (FSE, PON Ricerca e Innovazione 2014−2020, Azione I.1 "Dottorati Innovativi con caratter-

izzazione Industriale") funded the Ph.D. grant to A.V. A.M. acknowledges funding by Progetto CN 2—Spoke 2 Task 2.2.2—Plant multitrophic interactions underlying agroecosystem stability and resilience. This work benefited from access (ITA001) to CERM/CIRMMP, Italy Centre of Instruct-ERIC, a Landmark ESFRI project.

ABBREVIATIONS

CID	collision-induced dissociation
dHex	deoxy hexose;
dHexN	deoxy hexosamine
ESI FT-ICR MS	electrospray ionization Fourier transform ion cyclotron resonance mass spectrometry
Gal	galactose
GalA	galacturonic acid
GlcN	glucosamine
Hex	hexose
HexA	hexuronic acid
HexN	hexosamine
HexNAc	*N*-acetyl hexosamine
Kdo	3-deoxy-D-*manno*-octulosonic acid
Kdo5OMe	5-*O*-methyl-Kdo
Ko	D-*glycero*-D-*talo*-2-octulosonic acid
Ko5OMe	5-*O*-methyl-Ko
LOS	lipooligosaccharide
LPS	lipopolysaccharide
MALDI-TOF MS	matrix-assisted laser desorption/ionization time of flight mass spectrometry
OM	outer membrane
OS	core oligosaccharide after mild acid treatment
OS_{deAc}	fully deacylated core oligosaccharide
QuiN	quinovosamine
Rha	rhamnose
VLCFA	very long chain fatty acid

REFERENCES

(1) Trivedi, P.; Leach, J. E.; Tringe, S. G.; Sa, T.; Singh, B. K. Plant-microbiome interactions: from community assembly to plant health. *Nat. Rev. Microbiol.* **2020**, *18*, 607−621.
(2) Delaux, P. M.; Schornack, S. Plant evolution driven by interactions with symbiotic and pathogenic microbes. *Science* **2021**, *371*, No. eaba6605.
(3) Ferreira Filho, A. S.; Quecine, M. C.; Bogas, A. C.; Rossetto Pde, B.; Lima, A. O.; Lacava, P. T.; Azevedo, J. L.; Araújo, W. L. Endophytic Methylobacterium extorquens expresses a heterologous *β*-1,4-endoglucanase A (EglA) in Catharanthus roseus seedlings, a model host plant for Xylella fastidiosa. *World J. Microbiol. Biotechnol.* **2012**, *28*, 1475−1481.
(4) Knief, C.; Frances, L.; Vorholt, J. A. Competitiveness of diverse Methylobacterium strains in the phyllosphere of Arabidopsis thaliana and identification of representative models, including M. extorquens PA1. *Microb. Ecol.* **2010**, *60*, 440−452.
(5) Jourand, P.; Giraud, E.; Béna, G.; Sy, A.; Willems, A.; Gillis, M.; Dreyfus, B.; de Lajudie, P. Methylobacterium nodulans sp. nov., for a group of aerobic, facultatively methylotrophic, legume root-nodule-forming and nitrogen-fixing bacteria. *Int. J. Syst. Evol. Microbiol.* **2004**, *54*, 2269−2273.
(6) Sy, A.; Giraud, E.; Jourand, P.; Garcia, N.; Willems, A.; de Lajudie, P.; Prin, Y.; Neyra, M.; Gillis, M.; Boivin-Masson, C.; Dreyfus, B. Methylotrophic Methylobacterium bacteria nodulate and fix nitrogen in symbiosis with legumes. *J. Bacteriol.* **2001**, *183*, 214−220.
(7) Sy, A.; Timmers, A. C.; Knief, C.; Vorholt, J. A. Methylotrophic metabolism is advantageous for Methylobacterium extorquens during colonization of Medicago truncatula under competitive conditions. *Appl. Environ. Microbiol.* **2005**, *71*, 7245−7252.
(8) Ochsner, A. M.; Sonntag, F.; Buchhaupt, M.; Schrader, J.; Vorholt, J. A. Methylobacterium extorquens: methylotrophy and biotechnological applications. *Appl. Microbiol. Biotechnol.* **2015**, *99*, 517−534.
(9) Bhagat, N.; Raghav, M.; Dubey, S.; Bedi, N. Bacterial Exopolysaccharides: Insight into Their Role in Plant Abiotic Stress Tolerance. *J. Microbiol. Biotechnol.* **2021**, *31*, 1045−1059.
(10) Lim, C. K.; Villada, J. C.; Chalifour, A.; Duran, M. F.; Lu, H.; Lee, P. K. H. Designing and Engineering Methylorubrum extorquens AM1 for Itaconic Acid Production. *Front. Microbiol.* **2019**, *10*, 1027.
(11) Masi, M.; Réfregiers, M.; Pos, K. M.; Pagès, J. M. Mechanisms of envelope permeability and antibiotic influx and efflux in Gram-negative bacteria. *Nat. Microbiol.* **2017**, *2*, 17001.
(12) Henderson, J. C.; Zimmerman, S. M.; Crofts, A. A.; Boll, J. M.; Kuhns, L. G.; Herrera, C. M.; Trent, M. S. The Power of Asymmetry: Architecture and Assembly of the Gram-Negative Outer Membrane Lipid Bilayer. *Annu. Rev. Microbiol.* **2016**, *70*, 255−278.
(13) Belin, B. J.; Busset, N.; Giraud, E.; Molinaro, A.; Silipo, A.; Newman, D. K. Hopanoid lipids: from membranes to plant-bacteria interactions. *Nat. Rev. Microbiol.* **2018**, *16*, 304−315.
(14) Di Lorenzo, F.; Duda, K. A.; Lanzetta, R.; Silipo, A.; De Castro, C.; Molinaro, A. A Journey from Structure to Function of Bacterial Lipopolysaccharides. *Chem. Rev.* **2022**, *122*, 15767−15821.
(15) Llobet, E.; Martínez-Moliner, V.; Moranta, D.; Dahlström, K. M.; Regueiro, V.; Tomás, A.; Cano, V.; Pérez-Gutiérrez, C.; Frank, C. G.; Fernández-Carrasco, H.; Insua, J. L.; Salminen, T. A.; Garmendia, J.; Bengoechea, J. A. Deciphering tissue-induced Klebsiella pneumoniae lipid A structure. *Proc. Natl. Acad. Sci. U. S. A.* **2015**, *112*, E6369−E6378.
(16) Matsuura, M. Structural Modifications of Bacterial Lipopolysaccharide that Facilitate Gram-Negative Bacteria Evasion of Host Innate Immunity. *Front Immunol.* **2013**, *4*, 109.
(17) Bloem, K.; García-Vallejo, J. J.; Vuist, I. M.; Cobb, B. A.; van Vliet, S. J.; van Kooyk, Y. Interaction of the Capsular Polysaccharide A from Bacteroides fragilis with DC-SIGN on Human Dendritic Cells is Necessary for Its Processing and Presentation to T Cells. *Front Immunol.* **2013**, *4*, 103.
(18) Marchetti, R.; Forgione, R. E.; Fabregat, F. N.; Di Carluccio, C.; Molinaro, A.; Silipo, A. Solving the structural puzzle of bacterial glycome. *Curr. Opin. Struct. Biol.* **2021**, *68*, 74−83.
(19) Holst, O.; Thomas-Oates, J. E.; Brade, H. Preparation and structural analysis of oligosaccharide monophosphates obtained from the lipopolysaccharide of recombinant strains of Salmonella minnesota and Escherichia coli expressing the genus-specific epitope of Chlamydia lipopolysaccharide. *Eur. J. Biochem.* **1994**, *222*, 183−194.
(20) Nicolardi, S.; Joseph, A. A.; Zhu, Q.; Shen, Z.; Pardo-Vargas, A.; Chiodo, F.; Molinaro, A.; Silipo, A.; van der Burgt, Y. E. M.; Yu, B.; Seeberger, P. H.; Wuhrer, M. Analysis of Synthetic Monodisperse Polysaccharides by Wide Mass Range Ultrahigh-Resolution MALDI Mass Spectrometry. *Anal. Chem.* **2021**, *93*, 4666−4675.
(21) Di Lorenzo, F.; Palmigiano, A.; Al Bitar-Nehme, S.; Sturiale, L.; Duda, K. A.; Gully, D.; Lanzetta, R.; Giraud, E.; Garozzo, D.; Bernardini, M. L.; Molinaro, A.; Silipo, A. The Lipid A from Rhodopseudomonas palustris Strain BisA53 LPS Possesses a Unique Structure and Low Immunostimulant Properties. *Chemistry* **2017**, *23*, 3637−3647.
(22) Domon, B.; Costello, C. E. A systematic nomenclature for carbohydrate fragmentations in FAB-MS/MS spectra of glycoconjugates. *Glycoconjugate J.* **1988**, *5*, 397−409.
(23) D'Errico, G.; D'Ursi, A. M.; Marsh, D. Interaction of a peptide derived from glycoprotein gp36 of feline immunodeficiency virus and its lipoylated analogue with phospholipid membranes. *Biochemistry* **2008**, *47*, 5317−5327.
(24) Anthony, C. How half a century of research was required to understand bacterial growth on C1 and C2 compounds; the story of

https://doi.org/10.1021/jacsau.3c00025
JACS Au 2023, 3, 929−942

the serine cycle and the ethylmalonyl-CoA pathway. *Sci. Prog.* **2011**, *94*, 109−137.
(25) Chwastek, G.; Surma, M. A.; Rizk, S.; Grosser, D.; Lavrynenko, O.; Rucińska, M.; Jambor, H.; Sáenz, J. Principles of Membrane Adaptation Revealed through Environmentally Induced Bacterial Lipidome Remodeling. *Cell Rep.* **2020**, *32*, No. 108165.
(26) Rizk, S.; Henke, P.; Santana-Molina, C.; Martens, G.; Gnädig, M.; Nguyen, N. A.; Devos, D. P.; Neumann-Schaal, M.; Saenz, J. P. Functional diversity of isoprenoid lipids in Methylobacterium extorquens PA1. *Mol. Microbiol.* **2021**, *116*, 1064−1078.
(27) Silipo, A.; Vitiello, G.; Gully, D.; Sturiale, L.; Chaintreuil, C.; Fardoux, J.; Gargani, D.; Lee, H. I.; Kulkarni, G.; Busset, N.; Marchetti, R.; Palmigiano, A.; Moll, H.; Engel, R.; Lanzetta, R.; Paduano, L.; Parrilli, M.; Chang, W. S.; Holst, O.; Newman, D. K.; Garozzo, D.; D'Errico, G.; Giraud, E.; Molinaro, A. Covalently linked hopanoid-lipid A improves outer-membrane resistance of a Bradyrhizobium symbiont of legumes. *Nat. Commun.* **2014**, *5*, 5106.
(28) Di Lorenzo, F.; Palmigiano, A.; Duda, K. A.; Pallach, M.; Busset, N.; Sturiale, L.; Giraud, E.; Garozzo, D.; Molinaro, A.; Silipo, A. Structure of the Lipopolysaccharide from the Bradyrhizobium sp ORS285 rfaL Mutant Strain. *ChemistryOpen* **2017**, *6*, 541−553.
(29) Choma, A.; Zamłyńska, K.; Mazur, A.; Pastuszka, A.; Kaczyński, Z.; Komaniecka, I. Lipid A from Oligotropha carboxidovorans Lipopolysaccharide That Contains Two Galacturonic Acid Residues in the Backbone and Malic Acid A Tertiary Acyl Substituent. *Int. J. Mol. Sci.* **2020**, *21*, 7991.
(30) Choma, A.; Komaniecka, I.; Zebracki, K. Structure, biosynthesis and function of unusual lipids A from nodule-inducing and N2-fixing bacteria. *Biochim. Biophys. Acta, Mol. Cell Biol. Lipids* **2017**, *1862*, 196−209.
(31) Di Lorenzo, F.; Billod, J. M.; Martín-Santamaría, S.; Silipo, A.; Molinaro, A. Gram-Negative Extremophile Lipopolysaccharides: Promising Source of Inspiration for a New Generation of Endotoxin Antagonists. *Eur. J. Org. Chem.* **2017**, *2017*, 4055−4073.
(32) Roppel, J.; Mayer, H.; Weckesser, J. Identification of a 2,3-diamino-2,3-dideoxyhexose in the lipid A component of lipopolysaccharides of *Rhodopseudomonas viridis* and *Rhodopseudomonas palustris*. *Carbohydr. Res.* **1975**, *40*, 31−40.
(33) Choma, A.; Sowinski, P. Characterization of *Mesorhizobium huakuii* lipid A containing both D-galacturonic acid and phosphate residues. *Eur. J. Biochem.* **2004**, *271*, 1310−1322.
(34) Komaniecka, I.; Choma, A.; Lindner, B.; Holst, O. The structure of a novel neutral lipid A from the lipopolysaccharide of *Bradyrhizobium elkanii* containing three mannoses units in the backbone. *Chem. − Eur. J.* **2010**, *16*, 2922−2929.
(35) Pallach, M.; Di Lorenzo, F.; Facchini, F. A.; Gully, D.; Giraud, E.; Peri, F.; Duda, K. A.; Molinaro, A.; Silipo, A. Structure and inflammatory activity of the LPS isolated from *Acetobacter pasteurianus* CIP103108. *Int. J. Biol. Macromol.* **2018**, *119*, 1027−1035.
(36) Staudacher, E. Methylation—an uncommon modification of glycans. *Biol. Chem.* **2012**, *393*, 675−685.
(37) Wohlschlager, T.; Butschi, A.; Grassi, P.; Sutov, G.; Gauss, R.; Hauck, D.; Schmieder, S. S.; Knobel, M.; Titz, A.; Dell, A.; Haslam, S. M.; Hengartner, M. O.; Aebi, M.; Künzler, M. Methylated glycans as conserved targets of animal and fungal innate defense. *Proc. Natl. Acad. Sci. U. S. A.* **2014**, *111*, E2787−E2796.
(38) Vanacore, A.; Vitiello, G.; Wanke, A.; Cavasso, D.; Clifton, L. A.; Mahdi, L.; Campanero-Rhodes, M. A.; Solís, D.; Wuhrer, M.; Nicolardi, S.; Molinaro, A.; Marchetti, R.; Zuccaro, A.; Paduano, L.; Silipo, A. Lipopolysaccharide O-antigen molecular and supramolecular modifications of plant root microbiota are pivotal for host recognition. *Carbohydr. Polym.* **2022**, *277*, No. 118839.
(39) Vanacore, A.; Forgione, M. C.; Cavasso, D.; Nguyen, H. N. A.; Molinaro, A.; Saenz, J. P.; D'Errico, G.; Paduano, L.; Marchetti, R.; Silipo, A. Role of EPS in mitigation of plant abiotic stress: The case of Methylobacterium extorquens PA1. *Carbohydr. Polym.* **2022**, *295*, No. 119863.
(40) Pinisetty, D.; Moldovan, D.; Devireddy, R. The effect of methanol on lipid bilayers: an atomistic investigation. *Ann. Biomed. Eng.* **2006**, *34*, 1442−1451.
(41) Joo, H. J.; Ahn, S. H.; Lee, H. R.; Jung, S. W.; Choi, C. W.; Kim, M. S.; Bae, M. K.; Chung, I. K.; Bae, S. K.; Jang, H. O.; Yun, I. The effect of methanol on the structural parameters of neuronal membrane lipid bilayers. *Korean J. Physiol. Pharmacol.* **2012**, *16*, 255−264.
(42) Malajczuk, C. J.; Armstrong, B. I.; Stachura, S. S.; Mancera, R. L. Mechanisms of Interaction of Small Hydroxylated Cryosolvents with Dehydrated Model Cell Membranes: Stabilization vs Destruction. *J. Phys. Chem. B.* **2022**, *126*, 197−216.
(43) Patra, M.; Salonen, E.; Terama, E.; Vattulainen, I.; Faller, R.; Lee, B. W.; Holopainen, J.; Karttunen, M. Under the influence of alcohol: the effect of ethanol and methanol on lipid bilayers. *Biophys. J.* **2006**, *90*, 1121−1135.
(44) Burakowski, A.; Gliński, J. Hydration numbers of non-electrolytes from acoustic methods. *Chem. Rev.* **2012**, *112*, 2059−2081.
(45) Bakó, I.; Megyes, T.; Bálint, S.; Grósz, T.; Chihaia, V. Water-methanol mixtures: topology of hydrogen bonded network. *Phys. Chem. Chem. Phys.* **2008**, *10*, 5004−5011.
(46) Leontein, K.; Lindberg, B.; Lönngren, J. Assignment of absolute configuration of sugars by g.l.c. of their acetylated glycosides formed from chiral alcohols. *Carbohydr. Res.* **1978**, *62*, 359−362.
(47) Ceroni, A.; Maass, K.; Geyer, H.; Geyer, R.; Dell, A.; Haslam, S. M. GlycoWorkbench: a tool for the computer-assisted annotation of mass spectra of glycans. *J. Proteome Res.* **2008**, *7*, 1650−1659.
(48) Damerell, D.; Ceroni, A.; Maass, K.; Ranzinger, R.; Dell, A.; Haslam, S. M. The GlycanBuilder and GlycoWorkbench glycoinformatics tools: updates and new developments. *Biol. Chem.* **2012**, *393*, 1357−1362.
(49) Pither, M. D.; Illiano, A.; Pagliuca, C.; Jacobson, A.; Mantova, G.; Stornaiuolo, A.; Colicchio, R.; Vitiello, M.; Pinto, G.; Silipo, A.; Fischbach, M. A.; Salvatore, P.; Amoresano, A.; Molinaro, A.; Di Lorenzo, F. Bacteroides thetaiotaomicron rough-type lipopolysaccharide: The chemical structure and the immunological activity. *Carbohydr. Polym.* **2022**, *297*, No. 120040.
(50) Luchini, A.; Cavasso, D.; Radulescu, A.; D'Errico, G.; Paduano, L.; Vitiello, G. Structural Organization of Cardiolipin-Containing Vesicles as Models of the Bacterial Cytoplasmic Membrane. *Langmuir* **2021**, *37*, 8508−8516.
(51) Case, D. A.; Ben-Shalom, I. Y.; Brozell, S. R.; Cerutti, D. S.; et al. *AMBER 2018*; University of California: San Francisco, 2018.
(52) Roe, D. R.; Cheatham, T. E. PTRAJ and CPPTRAJ: Software for Processing and Analysis of Molecular Dynamics Trajectory Data. *J. Chem. Theory Comput.* **2013**, *9*, 3084−3095.

https://doi.org/10.1021/jacsau.3c00025
JACS Au 2023, 3, 929−942